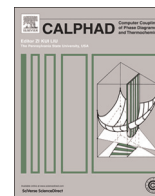




ELSEVIER

Contents lists available at ScienceDirect

# CALPHAD: Computer Coupling of Phase Diagrams and Thermochemistry

journal homepage: [www.elsevier.com/locate/calphad](http://www.elsevier.com/locate/calphad)

## Thermodynamic assessment of the cesium–oxygen system by coupling density functional theory and CALPHAD approaches



C. Guéneau\*, J.-L. Flèche

CEA Saclay, DEN, DPC, SCCME, F-91191 Gif-sur-Yvette, France

### ARTICLE INFO

#### Article history:

Received 17 September 2014

Received in revised form

13 February 2015

Accepted 18 February 2015

Available online 3 March 2015

#### Keywords:

Cesium oxides

Thermodynamics

Computational modeling

CALPHAD – first-principle calculations

Quasi-harmonic model

### ABSTRACT

The thermodynamic properties of cesium oxides were calculated by combining ab initio calculations at 0 K and a quasi-harmonic statistical thermodynamic model to determine the temperature dependency of the thermodynamic properties. In a second approach, the CALPHAD method was used to derive a model describing the Gibbs energy for all the cesium oxide compounds and the liquid phase of the cesium–oxygen system. For this approach, available experimental data in the literature was reviewed and it was concluded that only experimental thermodynamic data for  $\text{Cs}_2\text{O}$  are reliable. All these data together with the thermodynamic data calculated by combining ab initio and the statistical model were used to assess the Gibbs energy of all the phases of the cesium–oxygen system. A consistent thermodynamic model was obtained. The variation of the relative stability of the different oxides is discussed using structural and bond data for the oxides investigated by ab initio calculations. This work suggests that the melting point for  $\text{Cs}_2\text{O}_2$  reported in the literature (863 K) is probably overestimated and should be re-measured.

© 2015 Elsevier Ltd. All rights reserved.

### 1. Introduction

The fission of uranium–plutonium mixed oxide fuel in nuclear reactors produces many fission products and results in an increase in the oxygen potential of the fuel, which is a key thermodynamic data for nuclear fuels. Cesium is one of these major fission products. It can form ternary oxide phases such as  $\text{Cs}_x\text{U}_y\text{O}_z$ ,  $\text{Cs}_x\text{Mo}_y\text{O}_z$ , etc. in the fuel. When cesium combines with other elements, such as I, Te, O, it can be responsible for the chemical attack of steel claddings [1]. The fuelbase thermodynamic database is being developed in CEA since 2005 as a computational tool to perform thermodynamic calculations on mixed oxide fuels containing fission products to simulate the chemistry of the irradiated fuel [2–5]. In 2013, the TAF-ID project was launched to develop the same kind of database in frame of an international collaboration within the OECD/NEA [[www.oecd-nea.org/science/taf-id/](http://www.oecd-nea.org/science/taf-id/)]. The system Cs–O is a key system required to model and investigate important ternary systems (e.g., U–Cs–O, Cs–Te–O, Cs–Mo–O, etc.). This paper presents a review of available data in the literature and a thermodynamic assessment developed with the CALPHAD method on the basis of both selected experimental data coming from the literature as well as thermodynamic data for the cesium oxides calculated by combining ab initio calculations and a quasi-harmonic statistical model (present work). Experimental data

available in the literature are first reviewed. Then the method to calculate the thermodynamic functions for the different cesium oxides using ab initio calculations and the quasi-harmonic model is briefly described (complete method is discussed in Ref. [6]). Finally the thermodynamic assessment using all these data is presented.

### 2. Review of literature data

Numerous oxide compounds are reported to exist in the Cs–O system:  $\text{Cs}_7\text{O}$ ,  $\text{Cs}_4\text{O}$ ,  $\text{Cs}_7\text{O}_2$  (or  $\text{Cs}_{11}\text{O}_3$ ),  $\text{Cs}_3\text{O}$ ,  $\text{Cs}_2\text{O}$ ,  $\text{Cs}_2\text{O}_2$ ,  $\text{CsO}_2$ ,  $\text{Cs}_2\text{O}_3$ , and  $\text{CsO}_3$ . Thermodynamic and phase equilibria data available in the literature on the Cs–O system are summarized in Table 1. Thermodynamic data for cesium oxides were compiled and critically evaluated by Lamoreaux and Hildenbrand [7] and later by Cordfunke and Konings [8]. In this section, the available experimental data are reviewed.

#### 2.1 Phase diagram data

Only limited studies were undertaken on the Cs–O system by Rengade [9], Brauer [10] and Knights and Phillips [11]. The most recent version of the phase diagram published by Cordfunke and Konings [8] and later by Okamoto [22] was based on the experimental study performed by Knights and Phillips [11]. Among the different compounds, the existence of  $\text{Cs}_2\text{O}_3$  is not well established.

\* Corresponding author.

E-mail address: [christine.gueneau@cea.fr](mailto:christine.gueneau@cea.fr) (C. Guéneau).

**Table 1**  
Available experimental thermodynamic and phase diagram data on the Cs–O system

Type of data	Composition, temperature range (K)	Method	Reference	Remark
Phase diagram	Cs–Cs <sub>2</sub> O, 250–500 K	Thermal analysis	Rengade [9]	Not used
Phase diagram	Cs–Cs <sub>2</sub> O, 250–500 K	Thermal analysis	Brauer [10]	Selected
Phase diagram	Cs–CsO <sub>2</sub> , 250–500 K	Differential scanning calorimetry	Knights and Phillips [11]	Selected
Phase diagram	Melting point CsO <sub>2</sub>		Blumenthal [12]	Not used
Phase diagram	Melting point CsO <sub>2</sub>		Vol'nov [13]	Selected
Phase diagram	Melting point Cs <sub>2</sub> O	Differential thermal analysis, thermogravimetry, X-ray diffraction	Touzain [14]	Selected
Oxygen pressure	Cs <sub>2</sub> O <sub>2</sub> +CsO <sub>2</sub> , Cs <sub>2</sub> O <sub>2</sub> +Cs <sub>2</sub> O, 593–713 K	Manometer+balance	Berardinelli [15,16]	Selected
Oxygen potential	3.3–17 at% O, 773–973 K	Electromotive Force Measurement	Knights and Phillips [11]	Selected
Heat capacity	Cs <sub>2</sub> O, 5–350 K	Adiabatic calorimetry	Flotow and Osborne [17]	Selected
Oxygen pressure	Cs <sub>2</sub> O <sub>2</sub> , 573–613 K		Morris [18]	Not used
Cs pressure	Cs–Cs <sub>2</sub> O, 553–653 K	Membrane sensor	Arnol'dov [19]	Not used
Enthalpy of formation	Cs <sub>2</sub> O, 298.15 K	Solution calorimetry	Settle [20]	Selected
Enthalpy of formation	Cs <sub>2</sub> O, 298.15 K	Solution calorimetry	Beketov [39]	Not used

In the Cs–Cs<sub>2</sub>O part, an eutectic reaction (liquid=Cs bcc+Cs<sub>7</sub>O) was measured by Brauer [10] at 271 K and the compound Cs<sub>7</sub>O was found to melt congruently at 276 K. The measurements performed by Knights and Phillips [11] using a differential scanning calorimeter lead to some modifications of Brauer's version in the region from Cs<sub>7</sub>O to Cs<sub>7</sub>O<sub>2</sub>. An eutectic reaction (liquid=Cs<sub>7</sub>O+Cs<sub>4</sub>O) was measured by Knights and Phillips [11] at 262 K. Their observation of a transition at 262.7 K between 20 and 25 at% O implies that Cs<sub>7</sub>O<sub>2</sub> decomposes by a peritectic reaction into Cs<sub>7</sub>O and Cs<sub>3</sub>O. Cs<sub>4</sub>O was found to decompose at 326 K into liquid and Cs<sub>3</sub>O. And Cs<sub>3</sub>O was observed to decompose into liquid and Cs<sub>2</sub>O at 437 K. The melting point of Cs<sub>2</sub>O was found at 768 K by Touzain [14] using DTA.

The investigation of the Cs<sub>2</sub>O–CsO<sub>2</sub> region by Knights and Phillips [11] highlighted difficulties to obtain reproducible results on phase transitions due to a chemical interaction between the containment materials and samples. The melting points for Cs<sub>2</sub>O<sub>2</sub> and CsO<sub>2</sub> and the decomposition temperature of CsO<sub>3</sub> are quite uncertain and only indicative. The melting point of CsO<sub>2</sub> was estimated at 705 K by Blumenthal and Centerszwer [12] and later reported as 723 K by Vol'nov [13].

The largest uncertainties were on both the melting point of Cs<sub>2</sub>O<sub>2</sub> (863 K) and the decomposition of CsO<sub>3</sub> (343 K), which were reported on the phase diagrams successively by Knights and Phillips [11], Cordfunke and Konings [8]. In fact, the original paper with the measurements and the details on the method, cited by the above authors, could not be found in the literature.

To conclude, the phase equilibria are relatively well established in the Cs–Cs<sub>2</sub>O portion of the diagram. On the contrary, the Cs<sub>2</sub>O–O region is not well known and remains uncertain due to difficulties encountered during experimentation (e.g., chemical interaction between samples and crucibles).

## 2.2 Thermodynamic data

### 2.2.1. Oxygen and cesium potential data

The thermal decomposition of CsO<sub>2</sub> and Cs<sub>2</sub>O<sub>2</sub> oxides was investigated by Berardinelli [15] in the temperature range (633–723 K) using a manometer and a balance to determine the total pressure (O<sub>2</sub>) and oxygen to metal ratio. The overall composition of the samples fabricated from CsO<sub>2</sub> decomposition lied in the two-phase region (Cs<sub>2</sub>O<sub>2</sub>+CsO<sub>2</sub>) according to the reaction (2CsO<sub>2</sub>(s)=Cs<sub>2</sub>O<sub>2</sub>(s)+O<sub>2</sub>(g)). CsO<sub>2</sub> was observed to start to melt at 723 K in agreement with Vol'nov [13]. Measurements were carried out both below and above the melting temperature. Data measured in (Cs<sub>2</sub>O<sub>2</sub>+CsO<sub>2</sub>) by Berardinelli [15] compare very well with Morris's data [18]. From the measurements above the melt (733–773 K), two regions were proposed: a single liquid phase and a two-phase (liquid+Cs<sub>2</sub>O<sub>2</sub>) region. The liquidus composition in

this temperature range was estimated to be Cs<sub>2</sub>O<sub>3.32</sub>. Nevertheless the liquidus composition was found to be constant with temperature, which is not expected. The decomposition of Cs<sub>2</sub>O<sub>2</sub> according to the reaction (2Cs<sub>2</sub>O<sub>2</sub>(s)=2Cs<sub>2</sub>O(s)+O<sub>2</sub>(g)) was investigated over the temperature range (600–773 K) leading to sample composition ranging between Cs<sub>2</sub>O<sub>1.15</sub> and Cs<sub>2</sub>O<sub>1.94</sub> in the two-phase region (Cs<sub>2</sub>O+Cs<sub>2</sub>O<sub>2</sub>). Pressure data measured by Morris [18] are slightly lower than those of Berardinelli [15].

The measurements performed by Berardinelli in [15] on the thermal decomposition of Cs<sub>2</sub>O<sub>2</sub> and CsO<sub>2</sub> were later published in [16] in which experimental data measured above the melt were not reported.

Arnol'dov et al. [19] performed static measurements of total pressure (Cs) above Cs–Cs<sub>2</sub>O mixtures (with compositions ranging from 0 to 18.7 at% O). Pure cesium was taken as the standard state to determine activities. Pure cesium pressure data were found to be 15–20% higher than previous measurements. A comparison of data for pure cesium from Arnol'dov et al. [19] and from Hill and Gotoh [23] shows a large discrepancy between the two datasets.

Oxygen potentials in Cs–O liquids with 3.3–17 at% O at 773–973 K were determined by Knights and Phillips [11] from EMF measurements using ThO<sub>2</sub>–10 mol% Y<sub>2</sub>O<sub>3</sub> electrolyte. Cesium potentials were derived at 773 K using the Duhem–Margules equation. Knights and Phillips [11] have extrapolated oxygen and cesium potentials from 17 to 66 at% O as well as the Gibbs energy of formation of Cs<sub>2</sub>O, Cs<sub>2</sub>O<sub>2</sub>, and CsO<sub>2</sub> by combining their own measurements and data measured by Berardinelli and Kraus [16].

Knight and Phillips [11] compared their calculated Cs potentials using Gibbs–Duhem with experimental data derived by Arnol'dov et al. [19]. A good agreement was found except for the highest oxygen content (17.5 at% O). This disagreement could be due to a reaction with the reactor vessel according to Knight and Phillips [11]. As vapor pressure data for pure cesium from Arnol'dov et al. [19] are in disagreement with other data in the literature, the Cs potentials derived by Knight and Phillips [11] are preferred in the present work.

### 2.2.2. Enthalpy, entropy and heat capacity data

Cs<sub>2</sub>O is the only compound for which a reliable enthalpy of formation is available. In fact, the enthalpy of formation of Cs<sub>2</sub>O(s) was measured by Beketov [39], Rengade [9], and Settle et al. [20] at room temperature using solution-calorimetry from the enthalpy of reaction of Cs<sub>2</sub>O(s) with excess water from CsOH(aq). As recommended by Cordfunke and Konings [8], data measured by Settle et al. [20] is preferred:  $\Delta H_f^0$  (Cs<sub>2</sub>O at 298.15 K) =  $-345.98 \pm 1.17$  kJ/mol.

The heat capacity of Cs<sub>2</sub>O(s) was measured using adiabatic calorimetry from 5 to 350 K by Flotow and Osborne [17]. Thermodynamic data at room temperature and  $H^0$  (298.15 K)– $H^0$

(0) were obtained from these measurements:

$$C_p^0(\text{Cs}_2\text{O}) (\text{J} \cdot \text{mol}^{-1} \cdot \text{K}^{-1}) = 66.024 + 0.033461 \cdot (T/\text{K}),$$

$$S^0(\text{Cs}_2\text{O at 298.15 K}) = 146.87 \pm 0.44 (\text{J} \cdot \text{mol}^{-1} \cdot \text{K}^{-1})$$

The authors have extrapolated the heat capacity data up to 763 K and derived the Gibbs energy of formation using the enthalpy data of Settle et al. [20].

The Gibbs energy of formation of  $\text{Cs}_2\text{O}$ ,  $\text{Cs}_2\text{O}_2$ , and  $\text{CsO}_2$  was derived by Knights and Phillips [11] from oxygen and cesium potential data reported by Berardinelli and Kraus [16]:

$$\Delta G_f(\text{Cs}_2\text{O}_2) (\text{J} \cdot \text{mol}^{-1}) = -390,052 + 201.7 \cdot (T/\text{K}).$$

By the same method, Knights and Phillips [11] derived the Gibbs energy of formation of  $\text{CsO}_2$ :

$$\Delta G_f(\text{CsO}_2) (\text{J} \cdot \text{mol}^{-1}) = -233,145 + 153.65 \cdot (T/\text{K}).$$

Lindemer et al. [24] did their own assessment. Their data for  $\text{Cs}_2\text{O}_2$  and  $\text{CsO}_2$  are in disagreement with the oxygen potential data from Berardinelli and Kraus [16].

Thermodynamic data for  $\text{Cs}_2\text{O}$ ,  $\text{Cs}_2\text{O}_2$  and  $\text{CsO}_2$  compounds have been determined by Lamoreaux and Hildenbrand [7] on the basis of available experimental data as well as analogy with Na–O system. The authors have estimated the melting enthalpy of  $\text{Cs}_2\text{O}$ ,  $\text{Cs}_2\text{O}_2$ , and  $\text{CsO}_2$  too.

The selected experimental data for the thermodynamic assessment using the CALPHAD method are reported in Table 1.

### 3. Ab-initio calculations combined with a quasi-harmonic model

#### 3.1. Method to calculate the thermodynamic functions

The thermodynamic functions of the  $\text{Cs}_x\text{O}_{2y}$  compounds can be calculated starting from the free energy modeled at quasi-harmonic approximation level and with the assistance of ab initio calculations [6]. The advantage of this approach is that it does not require any parameter to perform the calculations except the symmetry group, the lattice parameters of the unit cell, and the atom position coordinates.

To determine the free energy of a crystal, containing  $N$  cells of  $n$  atoms per cell, the following three approximations are mainly used:

- i. The adiabatic approximation to calculate the cohesive energy of the crystal  $E_{\text{cohesive}}$  versus static pressure at zero kelvin, and correspondingly versus the equilibrium volume.
- ii. The harmonic approximation to calculate the  $3n$  vibration frequencies  $\nu_j(\vec{q})$  ( $j=1,3n$ ) for  $N$  values of wave vector  $\vec{q}$  in the first Brillouin zone. These  $3n$  frequencies dispersion branches are divided into three acoustic branches and  $(3n-3)$  optical branches. In order to make ab initio computations tractable, these vibration frequencies are calculated at the  $\Gamma$  point only ( $\vec{q} = 0$ ). For  $\vec{q} \neq 0$  we use the Debye model to determine the acoustic vibration frequencies and the Einstein model for the optical vibration frequencies. From  $E_{\text{cohesive}}(V)$  and the frequencies  $\nu_j(\vec{q}=0)$  ( $j=1,3n$ ) it is possible to construct the partition function of the crystal and deduce its free energy at temperature  $T$  by the statistical thermodynamic laws:

$$F = -E_{\text{cohesive}}(V) + Nk_B T \left[ \frac{9}{8} x_D + 3 \ln(1 - e^{-x_D}) - D(x_D) + \sum_{j=1}^{3n-3} \left( \frac{x_j}{2} + \ln(1 - e^{-x_j}) \right) \right] \quad (1)$$

where  $x_j = h\nu_j(0)/k_B T$ .  $D(x_D)$  is the Debye function with  $x_D = \Theta_D/T$  where  $\Theta_D$  is the Debye temperature.  $k_B$  and  $h$  are the Boltzmann and Planck constants, respectively. For an ideal isotropic crystal [6]  $\Theta_D$  is given by

$$\Theta_D = \frac{h}{k_B} \left( \frac{9}{4\pi V} \right)^{1/3} \left( \frac{3B}{\rho} \right)^{1/2} \left( \frac{1 - \sigma^0}{1 + \sigma^0} \right)^{1/2} \left( 1 + 2 \left( \frac{2 - 2\sigma^0}{1 - 2\sigma^0} \right)^{3/2} \right)^{-1/3} \quad (2)$$

$B$  is the bulk modulus,  $\rho$  is the density, and  $\sigma^0$  is the Poisson ratio (close to 0.33).

iii. To account for the thermal expansion while maintaining the simplicity of the harmonic model, quasi-harmonic approximation is used assuming that the vibration frequencies change with the volume of the unit cell:

$$pV = V \frac{dE_{\text{cohesive}}(V)}{dV} + Nk_B T \left[ \gamma_{\text{acoustic}} \left( \frac{9}{8} x_D + 3D(x_D) \right) + \gamma_{\text{optic}} \sum_{j=1}^{3n-3} \left( \frac{x_j}{2} + \frac{x_j}{e^{x_j} - 1} \right) \right] \quad (3)$$

where  $\gamma_{\text{acoustic}}$  and  $\gamma_{\text{optic}}$  are the Gruneisen coefficients. For an ideal isotropic crystal these Gruneisen coefficients are given by [6]

$$\gamma_{\text{acoustic}} = -\frac{2}{3} - \frac{1}{2} V \frac{d}{dV} \ln \left( \frac{d^2 E_{\text{cohesive}}(V)}{dV^2} \right) \quad (4)$$

$$\gamma_{\text{optic}} = \frac{1}{2} V \frac{d}{dV} \ln \left( \frac{d^2 E_{\text{cohesive}}(V)}{dV^{2/3}} \right) \quad (5)$$

The volume  $V$  is calculated iteratively for a given pressure and temperature, knowing  $E_{\text{cohesive}}(V)$  and the vibration frequencies at  $\Gamma$  point, as well as the Poisson ratio  $\sigma^0$  for the crystal to zero static pressure. From  $F(T, V)$  and  $pV$  we can calculate the entropy  $S = -(dF/dT)_V$ , the internal energy  $U = F + TS$ , the heat capacity at constant volume  $C_v = (dU/dT)_V$ , the bulk modulus  $B = -V(dp/dV)_T$ , the thermal expansion  $\alpha_p = (dp/dT)_V/B$ , and the heat capacity at constant pressure  $C_p = C_v + TVB\alpha^2$ . The calculation of the thermodynamic functions in the standard conditions is carried out with this approach, for the suboxides  $\text{Cs}_7\text{O}$ ,  $\text{Cs}_4\text{O}$ ,  $\text{Cs}_{11}\text{O}_3$ ,  $\text{Cs}_3\text{O}$ , the normal oxide  $\text{Cs}_2\text{O}$ , the peroxide  $\text{CsO}$  (or  $\text{Cs}_2\text{O}_2$ ), the superoxide  $\text{CsO}_2$ , and the cesium ozonide  $\text{CsO}_3$ .

#### 3.2. Results

The most studied cesium oxides, in the literature, from the point of view of their electronic structure calculation are  $\text{Cs}_2\text{O}$  [25–28],  $\text{Cs}_2\text{O}_2$  [25,27,28] and  $\text{CsO}_2$  [25,27–29]. Ab initio calculations were also performed for  $\text{Cs}_{11}\text{O}_3$ ,  $\text{Cs}_3\text{O}$ ,  $\text{CsO}_3$  in [28]. These results were obtained with different codes using the electronic density functional theory (DFT) with a plane-wave pseudo-potential method. The results of the formation enthalpy at 0 K obtained by these authors are reported in Table 5.

In the present work, our calculations were performed with the CASTEP code [30], which solves the electronic Schrödinger equation for a compound with periodic lattice, within the electronic

density functional theory (DFT) with a plane-wave pseudo-potential method. The tightly bound core electrons are represented by non local ultrasoft pseudo-potentials as proposed by Vanderbilt [31]. The exchange/correlation energies are calculated using the Perdew–Wang form of the generalized gradient approximation [32]. Due to the presence of oxygen, the cutoff energy is taken to 430 eV throughout all the calculations. The first Brillouin zone is approximated with finite sampling of k-points using the Monkhorst–Pack scheme [33].

Futhermore, when the electron spins of the ions are unpaired, the calculations are carried out with polarized spins. For CsO ( $\text{Cs}_2\text{O}_2$ ), which contains the peroxide ion  $\text{O}_2^{2-}$ , all the spins are paired. This is not the case for  $\text{CsO}_2$  and  $\text{CsO}_3$ , which contain an unpaired spin due to the presence of superoxide ion  $\text{O}_2^-$  and ozonide ion  $\text{O}_3^-$ , respectively. The spin polarization calculation with the symmetric group (I4/mmm) for  $\text{CsO}_2$  and (P21/c) for  $\text{CsO}_3$  opens an energy gap for  $\text{CsO}_3$ , but not for  $\text{CsO}_2$ . Experimental investigations and DFT calculations by Riyadi et al. [29] show that the symmetry group of  $\text{CsO}_2$  is lower than I4/mmm. To take into account the antiferromagnetic order proposed by the authors and open an energy gap,  $\text{CsO}_2$  material is studied with the I41/a symmetry group with unit cell dimensions corresponding to  $2a$ ,  $b$  and  $2c$  of the original cell.

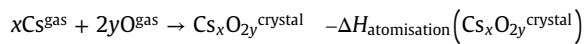
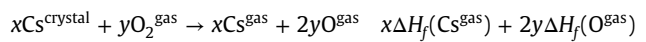
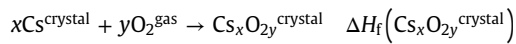
The set of parameters required for completing these ab initio calculations and the results obtained for the structure at zero pressure are listed in Table 2.

As shown in Table 2, the  $c$  parameter of the normal oxide  $\text{Cs}_2\text{O}$  is much larger than the lattice parameter of the reference structure, inducing a relative error of 23% on the equilibrium volume. In fact, the hexagonal unit cell of  $\text{Cs}_2\text{O}$  contains three triple layers Cs–O–Cs weakly bonded together through Van der Waals interactions [26]. Unfortunately, the correct long-range effect of such

interaction is absent from gradient corrected exchange–correlation functional in density–functional theory. To overcome this shortfall and obtain an improved result for the  $c$  parameter and volume (see Table 2), a special hybrid semi-empirical solution was applied. Such a modification allows the CASTEP code to introduce damped atom–pairwise dispersion corrections of the form  $C_6R^{-6}$  in the DFT formalism [35]. These corrections were also applied for  $\text{CsO}_3$  as a small increase in volume was initially calculated.

Using the total energy for cesium oxides for a given pressure and the energy of pure cesium and oxygen atoms as references, also calculated with the CASTEP code, we obtain the cohesive energy  $E_{\text{cohesive}}$  of the crystal as a function of the static pressure or the corresponding equilibrium volume  $V$ .

To calculate the standard enthalpy of formation  $\Delta H_f(T)$  we use Hess's law. Beside the reaction of formation of the cesium oxide from the pure components in their standard states, we consider the reaction of sublimation for cesium and dissociation of oxygen in atomic gas phase followed by the reaction of formation of the oxide from these gases, which is the reversed reaction of “atomisation”:



We obtain at temperature  $T$ :

$$\Delta H_f(\text{Cs}_x\text{O}_y^{\text{crystal}}) = x\Delta H_f(\text{Cs}^{\text{gas}}) + 2y\Delta H_f(\text{O}^{\text{gas}}) - \Delta H_{\text{atomisation}}(\text{Cs}_x\text{O}_y^{\text{crystal}}) \quad (6)$$

**Table 2**

Parameters and results of the ab initio calculations with the CASTEP Code. DFT lattice parameters (Å) and equilibrium volume of unit cell (Å<sup>3</sup>), in italic, at zero pressure, are compared to experimental data from Ref. [34].

Oxide	Symmetry group Exp. [34]	Magnetism	Monkhorst–Pack scheme	a (Å)		b (Å)		c (Å)		Volume(Å <sup>3</sup> )		Metal or insulator
				Exp. [34]	DFT calc.	Exp. [34]	DFT calc.	Exp. [34]	DFT calc.	Exp. [34]	DFT calc.	
Cs <sub>7</sub> O	Hex. P-6m2	no	8 8 12	16.393	<i>16.414</i>			9.193	<i>9.357</i>	2139.46	<i>2183.46</i>	Metal
											(2%)	
Cs <sub>4</sub> O	Orth. Pna21	no	6 5 9	16.833	<i>17.027</i>	20.569	<i>20.882</i>	12.400	<i>12.643</i>	4293.35	<i>4496.23</i>	Metal
											(5%)	
Cs <sub>11</sub> O <sub>3</sub>	Mono. P21/c	no	4 8 3	17.610	<i>17.880</i>	9.218	<i>9.377</i>	24.047	<i>24.466</i>	3842.55	<i>4035.98</i>	Metal
											(5%)	
Cs <sub>3</sub> O	Hex. P63/mcm	no	9 9 9	8.780	<i>8.899</i>			7.520	<i>7.627</i>	502.04	<i>523.17</i>	Metal
											(4%)	
Cs <sub>2</sub> O	Trig. R-3m	no	11 11 3	4.269	<i>4.330</i>			18.820	<i>22.491</i>	297.03	<i>365.20</i>	Insulator
											(23%)	
	with dispersion correction			4.232				18.74		290.57		
										(–2%)		
CsO	Orth. Immm	no	10 6 7	4.322	<i>4.460</i>	7.517	<i>7.644</i>	6.430	<i>6.495</i>	208.90	<i>221.43</i>	Insulator
											(6%)	
CsO <sub>2</sub>	Tetrag. I41/a (2a, b, 2c)	AFM	6 6 4	8.924	<i>9.031</i>			14.652	<i>14.906</i>	1166.85	<i>1215.72</i>	Insulator
											(4%)	
CsO <sub>3</sub>	Mono. P21/c	FM	7 7 5	6.709	<i>7.008</i>	6.244	<i>6.556</i>	8.997	<i>9.420</i>	323.56	<i>360.51</i>	Insulator
											(11%)	
	With dispersion correction			6.836		6.358	<i>6.358</i>	9.231		338.70		
										(5%)		

$\Delta H_f(\text{Cs}^{\text{gas}})$  and  $\Delta H_f(\text{O}^{\text{gas}})$  are known and tabulated.  $\Delta H_{\text{atomisation}}(\text{Cs}_x\text{O}_{2y}^{\text{crystal}})$  is given by the model

$$\begin{aligned} \Delta H_{\text{atomisation}}(\text{Cs}_x\text{O}_{2y}^{\text{crystal}}) &= E_{\text{cohesive}}(V) + V \frac{dE_{\text{coh}}(V)}{dV} + \frac{5}{2} n N k_B T \\ &\quad - N k_B T \left[ (\gamma_{\text{ac}} + 1) \left( \frac{9}{8} x_D + 3D(x_D) \right) + (\gamma_{\text{op}} + 1) \right. \\ &\quad \left. \sum_{j=1}^{3n-3} \left( \frac{x_j}{2} + \frac{x_j}{e^{x_j} - 1} \right) \right] \end{aligned} \quad (7)$$

The calculated enthalpy of formation  $\Delta H_f^0$ , entropy  $S^0$  and heat capacity at constant pressure  $C_p^0$  at 298.15 K and 1 atm for all the  $\text{Cs}_x\text{O}_{2y}^{\text{crystal}}$  compounds are compared with experimental and assessed data using CALPHAD in the next section (Table 5).

Concerning the heat capacity data at constant pressure, the following regression law is used:

$$C_p (\text{J} \cdot \text{mol}^{-1} \cdot \text{K}^{-1}) = k_0 + k_2 T^2 + k_1 T + k_{-2} T^{-2} \quad (8)$$

This mathematical function used in the CALPHAD models (Eq. (19)) is generally valid from 298.15 K to the melting point of the pure elements or compounds. In case of cesium with a low melting point at 300 K, the SGTE function from Dinsdale [36] used in our CALPHAD model is valid for  $T > 200$  K. Thus, we will consider that for all the compounds, our CALPHAD models are valid from temperatures higher than 200 K, which is consistent with the experimental phase diagram data [11] given for  $T > 200$  K.

Heat capacity data calculated with the quasi-harmonic model are compared with experimental data measured by Flotow and Osborne [17] from 5 to 350 K for the  $\text{Cs}_2\text{O}$  compound in Fig. 3(e). In fact, this is the only compound for which experimental heat capacity data are available. The agreement is good with a deviation of 1.6% at 300 K. Thus, we consider that our approach (DFT + quasi-harmonic model) is validated. Nevertheless, for this compound, we chose to fit existing experimental data instead of the theoretical data because we consider that these experimental data are more accurate. Data at higher temperature from the literature are extrapolated.

For the other compounds  $\text{Cs}_7\text{O}$ ,  $\text{Cs}_4\text{O}$ ,  $\text{Cs}_{11}\text{O}_3$ ,  $\text{Cs}_3\text{O}$ ,  $\text{Cs}_2\text{O}_2$ ,  $\text{CsO}_2$ , and  $\text{CsO}_3$  no experimental data exists. Therefore, the  $k_i$  coefficients were assessed by fitting quasi-harmonic model data. The results are shown in Fig. 3(a)–(d) and (f)–(h). The  $k_i$  coefficients are listed in Table 3 for all the compounds. A very good agreement is obtained for temperatures above 200 K.

A comparison between all data will be presented in the next section.

**Table 3**

Regression coefficients to fit the theoretical heat capacity data in  $\text{J} \cdot \text{mol}^{-1} \cdot \text{K}^{-1}$  of cesium oxides versus temperature at constant pressure valid from 298.15 K to the melting point. For  $\text{Cs}_2\text{O}$ , experimental data were used.

Oxide	$k_0$	$k_1$	$k_2$	$k_{-2}$
$\text{Cs}_7\text{O}$	0.18896318E+03	0.74629283E-01	0.11007908E-05	-0.78549294E+05
$\text{Cs}_4\text{O}$	0.11984977E+03	0.33404469E-01	0.95651960E-06	-0.10465812E+06
$\text{Cs}_{11}\text{O}_3$	0.33608049E+03	0.89345443E-01	0.23205005E-05	-0.31196982E+06
$\text{Cs}_3\text{O}$	0.63382374E+02	0.72948843E-01	-0.11304622E-05	-0.72192385E+05
$\text{Cs}_2\text{O}$	0.690158626E+02	0.2700182E-01	-0.37243959E-05	-0.8926800E+05
$\text{Cs}_2\text{O}_2$	0.84555089E+02	0.3563614E-01	-0.38732760E-05	-0.121432E+06
$\text{CsO}_2$	0.62655412E+02	0.22489574E-01	-0.48403552E-06	-0.76811847E+05
$\text{CsO}_3$	0.63382374E+02	0.72948843E-01	-0.11304622E-05	-0.72192385E+05

#### 4. CALPHAD assessment of the Cs–O system

The models to describe the Gibbs energies for all the phases are firstly described. Then the optimization procedure is explained and finally, the results are presented and compared to available experimental data and to calculated data for the compounds using DFT and the quasi-harmonic model.

##### 4.1. Models

All the Gibbs energies are referred to the Standard Element Reference (SER) state corresponding to  $H_i^{\text{SER}}$ , the enthalpy of the pure element in its stable state at 298.15 K and 1 atm.

##### 4.1.1. Pure elements

The Gibbs energy function  ${}^0G_i^\varphi(T) = G_i^\varphi(T) - H_i^{\text{SER}}$  for the element  $i$  in the phase  $\varphi$  is expressed as

$${}^0G_i^\varphi(T) = a + b \cdot T + c \cdot T \cdot \ln T + d_n \cdot T^n \quad (9)$$

with  $n=2, 3, -1$ .

The Gibbs energies for pure Cs and O were taken from Dinsdale [36].

##### 4.1.2. Liquid phase

A two-sublattice ionic liquid model  $(\text{Cs}^+)_P(\text{O}^{-2}, \text{Va}^{-Q}, \text{CsO}_2, \text{O})_Q$  was used to describe the liquid phase [37]. The model assumes that cations are in the first sublattice and that anions and neutral species mix in the second sublattice. Hypothetical charged vacancies ( $\text{Va}^{-Q}$ ) allow the neutrality of the system from the pure metal to the liquid oxides to be maintained.  $P$  and  $Q$  are the average charges of the first and second sublattices, respectively. For the Cs–O system,  $P$  and  $Q$  are equal to

$$P = 2y_{\text{O}^{2-}} + y_{\text{Va}^{-1}} \quad (10)$$

$$Q = 1 \quad (11)$$

where  $y_{\text{O}^{2-}}$  and  $y_{\text{Va}^{-1}}$  designate site fraction of oxygen and vacancies respectively in the second sublattice.

A first attempt was made to describe the liquid phase with the simplest sublattice model  $(\text{Cs}^+)_P(\text{O}^{-2}, \text{Va}^{-Q}, \text{O})_Q$  without associate species ( $\text{CsO}_2$ ). With this model, it was not possible to get a correct shape of the liquidus from  $\text{Cs}_2\text{O}$  to O. Thus, the  $(\text{CsO}_2)$  associate was added in the second sublattice. This species was preferred to  $(\text{Cs}_2\text{O}_2)$  due to the too large uncertainty on its melting point.

The Gibbs energy of the liquid phase is expressed as

$$G^{\text{liq}} = {}^{\text{ref}}G_{\text{liq}} + {}^{\text{id}}G_{\text{liq}} + {}^{\text{ex}}G_{\text{liq}} \quad (12)$$

**Table 4**  
Assessed thermodynamic parameters for the phases of the Cs–O system (J · mol<sup>-1</sup>).

Phase	Gibbs energy parameters (J · mol <sup>-1</sup> )	Reference
Liquid (Cs <sup>+</sup> ) <sub>l</sub> (O <sup>2-</sup> , Va <sup>-</sup> , CsO <sub>2</sub> , O) <sub>l</sub>	${}^0G_{(\text{Cs}^+)_2(\text{O}^{2-})}^{\text{liq}} = {}^0G^{\text{Cs}_2\text{O}} + 25,799.2 - 33.592632 T$	This work
	${}^0G_{(\text{Cs}^+)(\text{Va}^-)}^{\text{liq}}$	[36]
	${}^0G_{(\text{CsO}_2)}^{\text{liq}} = {}^0G^{\text{CsO}_2} + 24,942 - 32 T$	This work
	${}^0G_{(\text{O})}^{\text{liq}}$	[36]
	$L_{(\text{Cs}^+)(\text{O}^{2-}, \text{Va})}^0 = -29,927 + 5.4535 T$	This work
	$L_{(\text{Cs}^+)(\text{O}^{2-}, \text{Va})}^1 = -4978 + 9.926 T$	This work
	$L_{(\text{Cs}^+)(\text{O}^{2-}, \text{Va})}^2 = 6971$	This work
	$L_{(\text{Cs}^+)(\text{O}^{2-}, \text{CsO}_2)}^0 = 7000$	This work
Cs <sub>7</sub> O	${}^0G^{\text{Cs}_7\text{O}} = -400,474 + 663.75459 T - 188.96318 T \ln(T) - 0.037314641 T^2$ $- 1.8346513 \times 10^{-7} T^3 + 39275 T^{-1}$	This work
	${}^0G^{\text{Cs}_4\text{O}} = -376,829 + 449.05376 T - 119.84977 T \ln(T) - 0.016702234 T^2$ $- 1.5941993 \times 10^{-7} T^3 + 52329 T^{-1}$	This work
Cs <sub>7</sub> O <sub>2</sub>	${}^0G^{\text{Cs}_7\text{O}_2} = -750,000 + 843.9 T - 216.051744 T \ln(T) - 0.028718178 T^2$ $- 2.48625 \times 10^{-7} T^3 + 100,276 T^{-1}$	This work
Cs <sub>3</sub> O	${}^0G^{\text{Cs}_3\text{O}} = -371,929 + 388.84685 T - 95.926195 T \ln(T) - 0.012825603 T^2$ $- 1.3849564 \times 10^{-7} T^3 + 42,364 T^{-1}$	This work
Cs <sub>2</sub> O	${}^0G^{\text{Cs}_2\text{O}} = -368,025 + 323.73258 T - 69.0158626 T \ln(T) - 0.0135009113 T^2$ $+ 6.2073265 \times 10^{-7} T^3 + 44,634 T^{-1}$	This work
Cs <sub>2</sub> O <sub>2</sub>	${}^0G^{\text{Cs}_2\text{O}_2} = -417,219 + 362 T - 84.555089 T \ln(T) - 0.01781807 T^2$ $+ 6.45545997 \times 10^{-7} T^3 + 60,716 T^{-1}$	This work
CsO <sub>2</sub>	${}^0G^{\text{CsO}_2} = -261,350 + 263.5 T - 62.655412 T \ln(T) - 0.011244787 T^2$ $+ 8.0672586 \times 10^{-8} T^3 + 38,406 T^{-1}$	This work
CsO <sub>3</sub>	${}^0G^{\text{CsO}_3} = -295,000 + 278 T - 63.382374 T \ln(T) - 0.036474421 T^2$ $+ 1.8841036 \times 10^{-7} T^3 + 36,096 T^{-1}$	This work

with

$$\text{ref}G^{\text{liq}} = y_{\text{O}^{2-}} {}^0G_{(\text{Cs}^+)_2(\text{O}^{2-})}^{\text{liq}} + y_{\text{Va}} {}^0G_{(\text{Cs}^+)(\text{Va}^-)}^{\text{liq}} + y_{\text{CsO}_2} {}^0G_{(\text{CsO}_2)}^{\text{liq}} + y_{\text{O}} {}^0G_{(\text{O})}^{\text{liq}} \quad (13)$$

$$\text{id}G^{\text{liq}} = QRT \left( y_{\text{O}^{2-}} \ln y_{\text{O}^{2-}} + y_{\text{Va}} \ln y_{\text{Va}} + y_{\text{CsO}_2} \ln y_{\text{CsO}_2} + y_{\text{O}} \ln y_{\text{O}} \right) \quad (14)$$

$$\text{ex}G^{\text{liq}} = y_{\text{O}^{2-}} y_{\text{Va}} L_{(\text{Cs}^+)(\text{O}^{2-}, \text{Va})}^{\text{liq}} + y_{\text{O}^{2-}} y_{\text{CsO}_2} L_{(\text{Cs}^+)(\text{O}^{2-}, \text{CsO}_2)}^{\text{liq}} + y_{\text{O}^{2-}} y_{\text{CsO}_2} L_{(\text{Cs}^+)(\text{CsO}_2, \text{O})}^{\text{liq}} \quad (15)$$

with

$$L_{(\text{Cs}^+)(\text{O}^{2-}, \text{Va})}^{\text{liq}} = L_{(\text{Cs}^+)(\text{O}^{2-}, \text{Va})}^0 + (y_{\text{O}^{2-}} - y_{\text{Va}}) L_{(\text{Cs}^+)(\text{O}^{2-}, \text{Va})}^1 + (y_{\text{O}^{2-}} - y_{\text{Va}})^2 L_{(\text{Cs}^+)(\text{O}^{2-}, \text{Va})}^2 \quad (16)$$

$$L_{(\text{Cs}^+)(\text{O}^{2-}, \text{CsO}_2)}^{\text{liq}} = L_{(\text{Cs}^+)(\text{O}^{2-}, \text{CsO}_2)}^0 \quad (17)$$

$$L_{(\text{Cs}^+)(\text{CsO}_2, \text{O})}^{\text{liq}} = L_{(\text{Cs}^+)(\text{CsO}_2, \text{O})}^0 \quad (18)$$

where the interaction coefficients  $L^i$  with  $i=0, 1, 2$  can have a linear dependence with temperature. Interaction parameters between (O<sup>2-</sup>, Va), (O<sup>2-</sup>, CsO<sub>2</sub>) and (CsO<sub>2</sub>, O) species are assessed to describe the liquidus in (Cs–Cs<sub>2</sub>O), (Cs<sub>2</sub>O–CsO<sub>2</sub>) and (CsO<sub>2</sub>–O) composition ranges, respectively.

#### 4.1.3. Solid oxide compounds

Cs<sub>7</sub>O, Cs<sub>4</sub>O, Cs<sub>7</sub>O<sub>2</sub>, Cs<sub>3</sub>O, Cs<sub>2</sub>O, Cs<sub>2</sub>O<sub>2</sub>, CsO<sub>2</sub> and CsO<sub>3</sub> oxides are described as stoichiometric compounds. The Gibbs energy function for a Cs<sub>*n*</sub>O<sub>*m*</sub> compound referred to the standard enthalpy of the elements is expressed by

$${}^0G_i^{\text{Cs}_n\text{O}_m}(T) - n \cdot H_{\text{Cs}}^{\text{SER}} - m \cdot H_{\text{O}}^{\text{SER}} = a + b \cdot T + c \cdot T \cdot \ln T + d_n \cdot T^n \quad (19)$$

with  $n=2, 3, -1$ . For Cs<sub>7</sub>O<sub>2</sub> compound data, which was reported on the phase diagram and chosen in the CALPHAD assessment, the DFT calculations were performed on Cs<sub>11</sub>O<sub>3</sub> and then rescaled by multiplying by a factor of (9/14).

#### 4.1.4. Gas phase

The gas is described as an ideal mixture of the following species:

(Cs, Cs<sub>2</sub>, Cs<sub>2</sub>O, Cs<sub>2</sub>O<sub>2</sub>, O, O<sub>2</sub>, O<sub>3</sub>)

The Gibbs energy is expressed by

$$G^{\text{gas}} = \sum_i y_i \left[ {}^0G_i^{\text{gas}} - \sum_j b_{ij} H_j^{\text{SER}} + RT \ln y_i \right] + RT \ln \left( \frac{p}{p_0} \right) \quad (20)$$

where  $y_i$  are the constituent fractions. Their sum is thus unity.  $b_{ij}$  is the number of atoms  $j$  in the species  $i$ . The standard pressure  $p_0$  is set to 10<sup>5</sup> Pa. The partial pressure of species  $i$ ,  $p_i$  is related to the constituent fraction by  $p_i = y_i p$  where  $p$  is the total pressure.

The thermodynamic parameters were taken from the SGTE substance database [38].

**Table 5**

Enthalpy of formation ( $\Delta H_f^0$ ), standard entropy ( $S^0$ ) and heat capacity ( $C_p^0$ ) data at 298.15 K for all the cesium oxide compounds. Comparison between calculated data (DFT and CALPHAD calculations from this work) and results coming from the literature (experiments, DFT and reviews).

Oxide	$\Delta H_f^0$ 298.15 K (kJ/mol)	$S^0$ 298.15 K (J mol <sup>-1</sup> K <sup>-1</sup> )	$C_p^0$ 298.15 K (J mol <sup>-1</sup> K <sup>-1</sup> )	Method reference
Cs <sub>7</sub> O	–299.8	617.3	210.5	DFT – this work
	– <b>340.5</b>	<b>624.6</b>	<b>210.4</b>	CALPHAD – this work
Cs <sub>4</sub> O	–298.2	304.3	136.4	DFT – this work
	– <b>339.2</b>	<b>364.2</b>	<b>128.7</b>	CALPHAD – this work
Cs <sub>7</sub> O <sub>2</sub> from Cs <sub>11</sub> O <sub>3</sub>	–576.0	545.0	231.2	DFT – this work
	– <b>682.3</b>	<b>621.4</b>	<b>231.1</b>	CALPHAD – this work
Cs <sub>3</sub> O	–296.5	237.0	106.8	DFT – this work
	–370.3 (0 K)	–	–	DFT – Jain[28]
	– <b>341.9</b>	<b>261.8</b>	<b>102.7</b>	CALPHAD – this work
Cs <sub>2</sub> O	–367.1	157.3	74.8	DFT – this work
	–350.8 (0 K)	–	–	DFT – Jain [28]
	–352.2 (0 K)	–	–	DFT – Brillant [27]
	–	146.9	76	Exp. – Flotow [17]
	–346.0	146.9	–	Rev. – Cordfunke [8]
	–346.0	146.9	76	Rev. – SGTE [38]
	–346.0	146.9	–	Rev. – Lamoreaux[7]
	–346.0	146.7	–	Exp. – Settle [20]
	–348.4	114.6	–	Exp. – Knights [11]
	– <b>346.0</b>	<b>146.9</b>	<b>75.7</b>	CALPHAD – this work
	Cs <sub>2</sub> O <sub>2</sub>	–391.8	163.7	111.0
–524.1 (0 K)		–	–	DFT – Jain [28]
–516.2 (0 K)		–	–	DFT – Brillant [27]
–440.0		173.6	–	Rev. – Cordfunke [8]
–440.0		180	95.0	Rev. – SGTE [38]
–497.6		144.3	–	Rev. – Lamoreaux [7]
–386.5		213.3	–	Exp. – Knights [11]
– <b>390.0</b>		<b>215.4</b>	<b>93.5</b>	CALPHAD – this work
CsO <sub>2</sub>	–252.8	147.5	68.2	DFT – this work
	–388.6 (0 K)	–	–	DFT – Jain [28]
	–351.2 (0 K)	–	–	DFT – Brillant [27]
	–233.1	136.5	–	Rev. – Cordfunke [8]
	–286.2	142.0	78.9	Rev. – SGTE [38]
	–286.2	139.8	–	Rev. – Lamoreaux [7]
	–234.9	171.2	–	Exp. – Knights [11]
	– <b>241.4</b>	<b>163.2</b>	<b>68.45</b>	CALPHAD – this work
CsO <sub>3</sub>	–284.0	144.7	84.3	DFT – this work
	–200.7 (0 K)	–	–	DFT – Jain [28]
	– <b>272.6</b>	<b>168.6</b>	<b>84.2</b>	CALPHAD – this work

#### 4.2. Optimization method

The optimized Gibbs energy parameters for all the phases are reported in Table 4.

As reported in Section 3.2, in a first step, the  $c$  and  $d_n$  coefficients entering the Gibbs energy functions  ${}^0G_i^{Cs_nO_m}$  for the oxide compounds (Eq. (9)) were fixed by fitting the calculated values from ab initio calculations combined with the quasi-harmonic thermodynamic model (Section 3, Table 3) for Cs<sub>7</sub>O, Cs<sub>4</sub>O, Cs<sub>3</sub>O, Cs<sub>7</sub>O<sub>2</sub>, Cs<sub>2</sub>O<sub>2</sub>, CsO<sub>2</sub>, and CsO<sub>3</sub> oxides. For Cs<sub>2</sub>O compound, experimental data were preferred for the fit.

In a second step, the enthalpy and entropy terms for solid Cs<sub>2</sub>O were assessed. The  $a$  and  $b$  coefficients in the Gibbs energy functions  ${}^0G_i^{Cs_nO_m}$  in Eq. (9) were initialized considering the experimental enthalpy of formation and standard entropy at 298.15 K from respectively Settle et al. [20] and Flotow and Osborne [17]. For liquid Cs<sub>2</sub>O, the melting enthalpy estimated by Lamoreaux and Hildenbrand [7] was utilized.

In a third step, interaction parameters in the liquid between (O<sup>2-</sup> and Va) species were assessed to fit experimental oxygen potential data measured in the Cs–Cs<sub>2</sub>O region by Knights and

Phillips [11]. Then the  $a$  and  $b$  coefficients in the Gibbs energy functions  ${}^0G_i^{Cs_nO_m}$  in Eq. (9) for Cs<sub>7</sub>O, Cs<sub>4</sub>O, Cs<sub>7</sub>O<sub>2</sub>, and Cs<sub>3</sub>O were assessed to fit the phase diagram data in the Cs–Cs<sub>2</sub>O region.

In a fourth step, the region between Cs<sub>2</sub>O and O was investigated. The  $a$  and  $b$  coefficients in the Gibbs energy functions  ${}^0G_i^{Cs_nO_m}$  in Eq. (9) for Cs<sub>2</sub>O<sub>2</sub> and CsO<sub>2</sub> were assessed using oxygen pressure data measured by Berardinelli [15,16]. As starting value, the melting enthalpy estimated by Lamoreaux and Hildenbrand [7] was taken for the Gibbs energy of CsO<sub>2</sub> liquid.

Finally, in a last step, interaction parameters in the liquid between (O<sup>2-</sup>, CsO<sub>2</sub>) and (CsO<sub>2</sub>, O) were assessed to fit the scarce phase diagram data in the Cs<sub>2</sub>O–O region. These experimental data correspond only to the melting points for Cs<sub>2</sub>O<sub>2</sub>, CsO<sub>2</sub>, and the decomposition temperature for CsO<sub>3</sub>. Oxygen potential data measured by Berardinelli [15] above the melt were also incorporated. It was not possible to lead to a good agreement for the melting point of Cs<sub>2</sub>O<sub>2</sub>, but as mentioned previously, the melting point for this compound is quite uncertain.

#### 4.3. Results and discussion

The calculated phase diagrams without and with the gas phase are presented in Fig. 1(a) and (b), respectively.

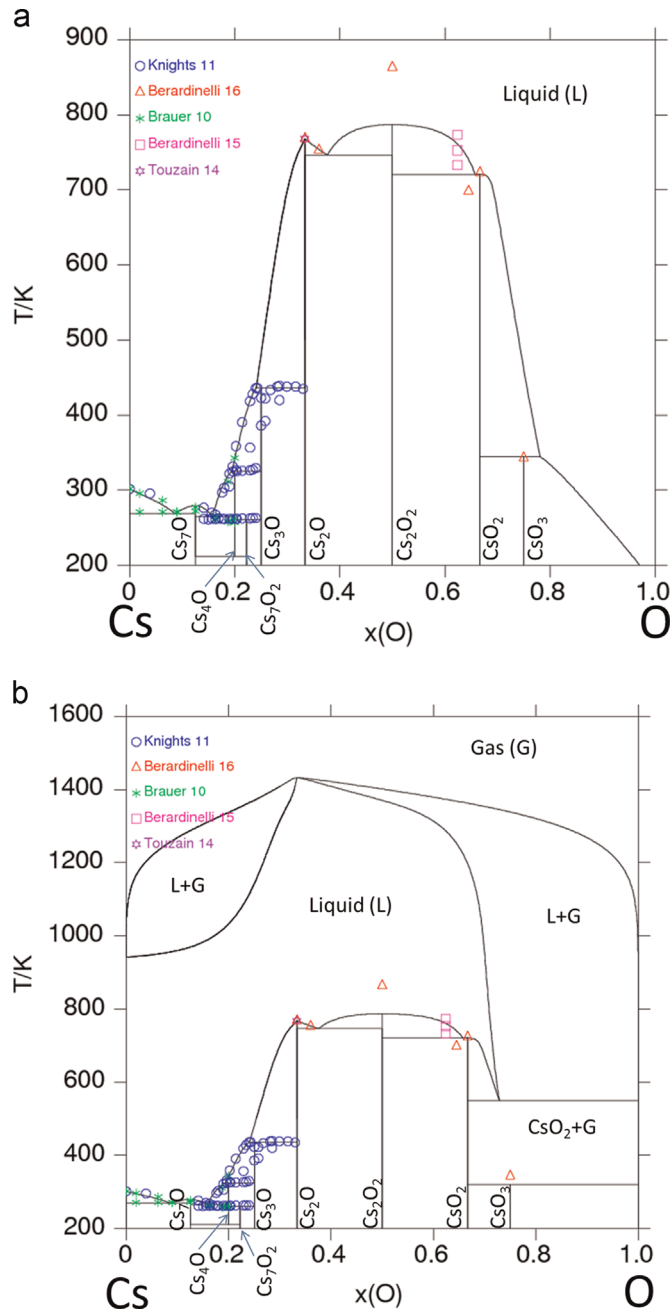


**Fig. 1.** Calculated phase diagram of the Cs–O system (a) without gas phase (b) with gas phase.

A good agreement between the calculated phase diagram and the experimental data is found in the Cs–Cs<sub>2</sub>O region, for which experimental information is available.

As mentioned in the literature review, the phase diagram from Cs<sub>2</sub>O composition to pure oxygen is quite uncertain due to experimental issues. There are no liquidus data except the roughly value coming from Berardinelli [15]. Only melting point values for Cs<sub>2</sub>O, Cs<sub>2</sub>O<sub>2</sub>, CsO<sub>2</sub> and decomposition temperature for CsO<sub>3</sub> are available in the literature. In the assessment, it was not possible to reproduce the melting point of Cs<sub>2</sub>O<sub>2</sub> (863 K). By increasing the weighting factor to fit the melting point for Cs<sub>2</sub>O<sub>2</sub>, at 863 K, the compound became unstable at room temperature and pressure data and thermodynamic data at room temperature were not well reproduced.

Because the original paper on the determination of this melting point for Cs<sub>2</sub>O<sub>2</sub> compound could not be found, no information is

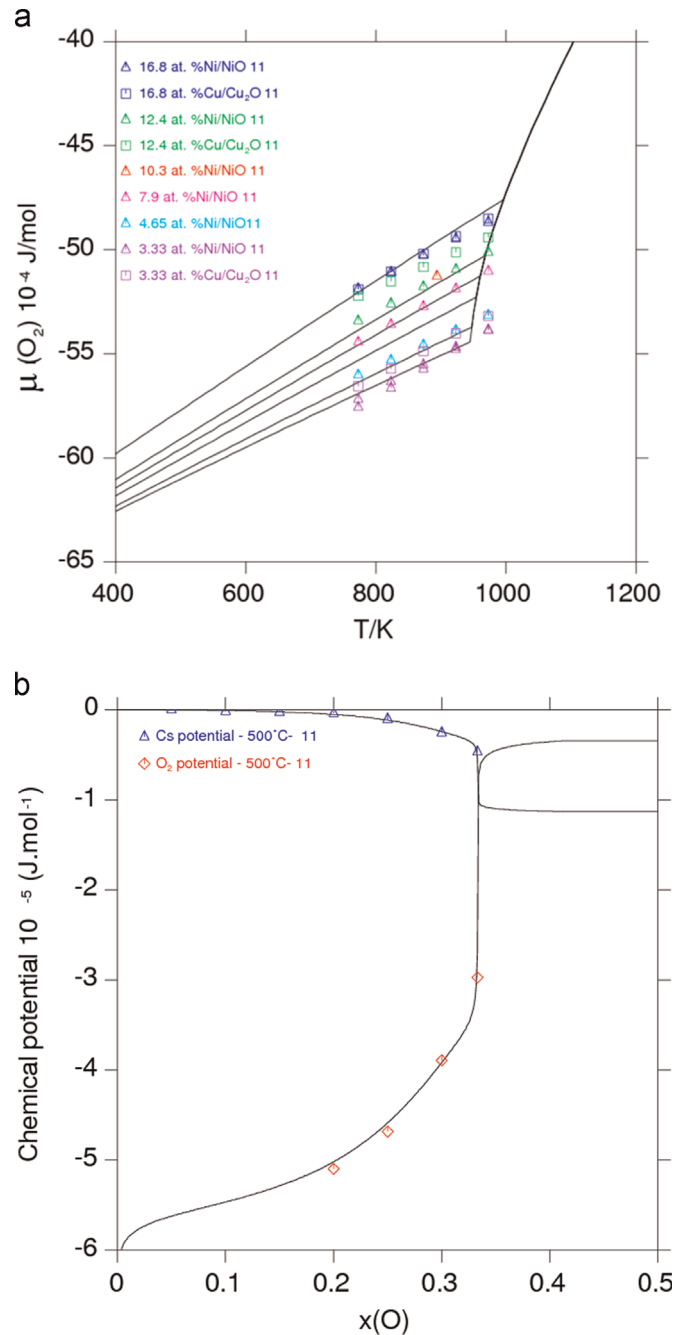


**Fig. 2.** (a) Calculated oxygen potential ( $\text{J} \cdot \text{mol}^{-1}$ ) versus temperature for 3.33, 4.65, 7.9, 10.3, 12.4, 16.8 at% O; (b) calculated oxygen and cesium chemical potential ( $\text{J} \cdot \text{mol}^{-1}$ ) versus oxygen atomic fraction at 773 K; comparison with experimental data measured by Knights and Phillips [11].

available on this measurement, which is reported in previous papers. Thus, this value is considered as quite uncertain. Moreover, the most stable compound in the Cs–O system is Cs<sub>2</sub>O, which thus should have the highest melting point, instead of Cs<sub>2</sub>O<sub>2</sub>. Thus, a largest weighting factor was attributed to thermodynamic data on solid Cs<sub>2</sub>O<sub>2</sub>, which was derived from both ab initio and quasi-harmonic model and from vapor pressure measurements above the (Cs<sub>2</sub>O+Cs<sub>2</sub>O<sub>2</sub>) and (Cs<sub>2</sub>O<sub>2</sub>+CsO<sub>2</sub>) regions.

Fig. 2(a) compares calculated oxygen potential data versus temperature in the liquid (Cs–Cs<sub>2</sub>O region) to the experimental measurements by Knights and Phillips [11]. Both calculated oxygen and cesium chemical potential data versus oxygen composition at 773 K are compared to data from Knights and Phillips [11]

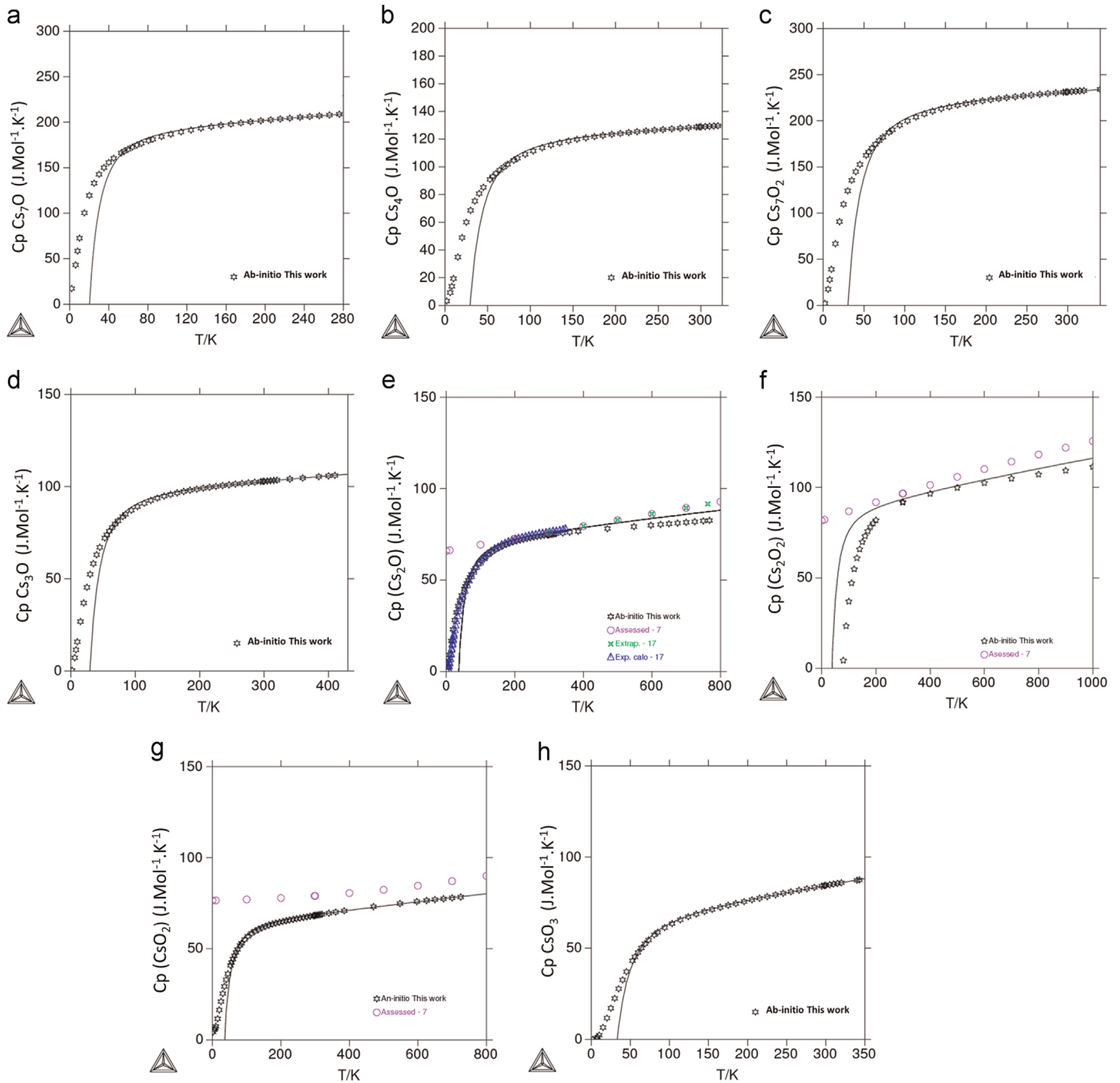


**Fig. 3.** Calculated heat capacity data versus temperature using the regression laws reported in Table 3 and also used in the CALPHAD models for (a)  $\text{Cs}_7\text{O}$ , (b)  $\text{Cs}_4\text{O}$ , (c)  $\text{Cs}_7\text{O}_2$ , (d)  $\text{Cs}_3\text{O}$ , (e)  $\text{Cs}_2\text{O}$ , (f)  $\text{Cs}_2\text{O}_2$ , (g)  $\text{CsO}_2$ , (h)  $\text{CsO}_3$  and comparison with the data calculated using the DFT and quasi-harmonic model (black points) as well as with data coming from the literature.

in Fig. 2(b). A good agreement is obtained for both oxygen and cesium chemical potential, which gives a good confidence in the thermodynamic model for the Cs– $\text{Cs}_2\text{O}$  region.

Table 3 lists the Gibbs energy coefficients for the compounds and the heat capacity, which were derived from ab initio calculations and quasi-harmonic model; except for  $\text{Cs}_2\text{O}$ , which was directly fitted from experimental data. Heat capacity data for all compounds are presented in Fig. 3(a)–(h). The comparison with data from the literature is only possible for  $\text{Cs}_2\text{O}$ ,  $\text{Cs}_2\text{O}_2$ , and  $\text{CsO}_2$ . Experimental data only exist for the  $\text{Cs}_2\text{O}$  compound. For this compound, the agreement between the model (ab-initio+quasi-harmonic approximation) and the experimental data measured by Flotow and Osborne [17] below 350 K is good, which gives

confidence to the results obtained by our approach. The estimation by Lamoreaux and Hildenbrand [7] is only valid for temperatures above 300 K and leads to systematically higher values for heat capacities at high temperature for  $\text{Cs}_2\text{O}$ ,  $\text{Cs}_2\text{O}_2$ , and  $\text{CsO}_2$ . As no experimental data are available in this temperature range, our calculated functions using our approach (ab initio+quasi-harmonic approximation) are preferred.

Once the heat capacity functions were fixed for all the compounds, the enthalpy and entropy terms for  $\text{Cs}_2\text{O}$  were assessed to fit experimental data from Settle et al. [20] for the enthalpy of formation and from Flotow and Osborne [17] for the standard entropy at 298.15 K. Then the enthalpy and entropy terms for  $\text{Cs}_2\text{O}_2$  and  $\text{CsO}_2$  were assessed to fit oxygen pressure data

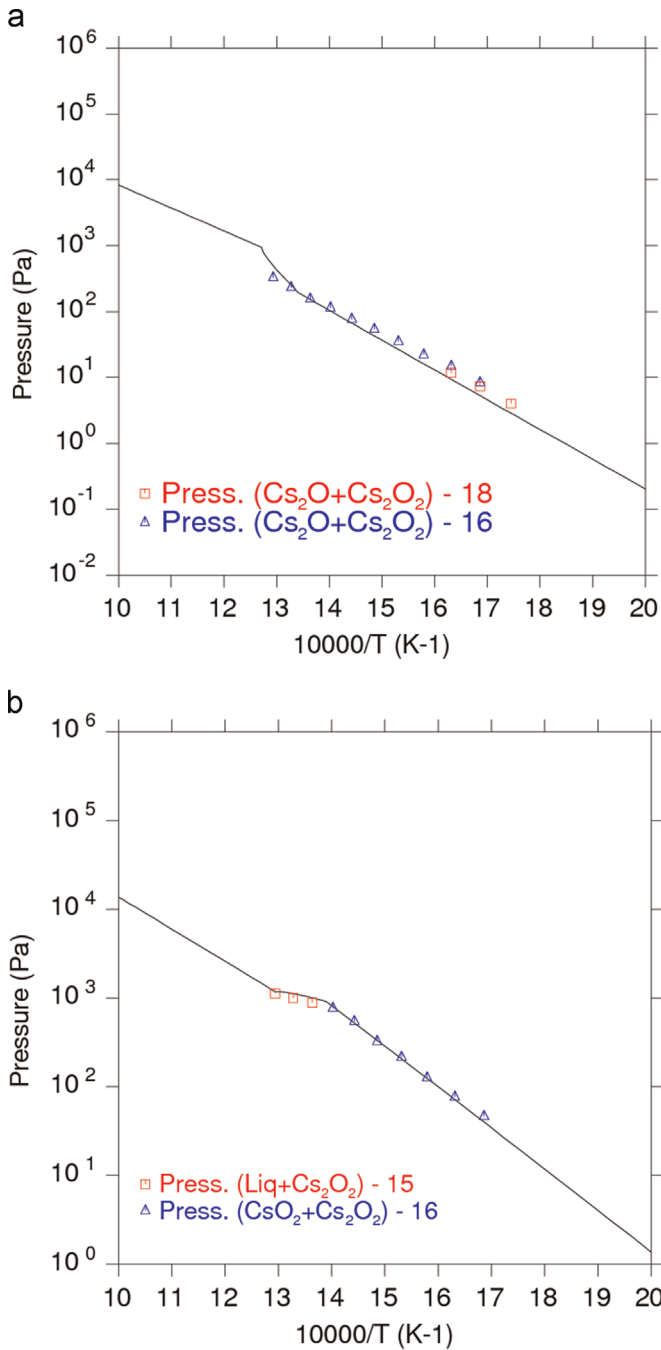


**Fig. 4.** Calculated pressure data versus temperature above (a)  $(\text{Cs}_2\text{O}+\text{Cs}_2\text{O}_2)$  and (b)  $(\text{Cs}_2\text{O}_2+\text{Cs}_2\text{O}_2)$  regions, compared to the experimental data from Berardinelli [15,16] and Morris [18].

measured by Berardinelli [15,16] above the  $(\text{Cs}_2\text{O}+\text{Cs}_2\text{O}_2)$  and  $(\text{Cs}_2\text{O}_2+\text{Cs}_2\text{O}_2)$  regions. As shown in Fig. 4(a) and (b), the agreement is very good between the calculated and experimental pressure data.

For the liquid in the  $\text{Cs}_2\text{O}-\text{O}$  region, melting enthalpy data estimated by Lamoreaux and Hildenbrand [7] for  $\text{Cs}_2\text{O}$  and  $\text{CsO}_2$  were used to determine the Gibbs energy functions for these compositions in the liquid. Then interaction parameters between  $(\text{O}^{2-}, \text{CsO}_2)$  and  $(\text{CsO}_2, \text{O})$  were assessed to try to reproduce the very tentative phase diagram proposed by Knights and Phillips [11]. Oxygen pressure data measured in the melt close to the  $\text{CsO}_2$  composition were found in [15]. It is surprising to note that these measurements were not reported in the published work by

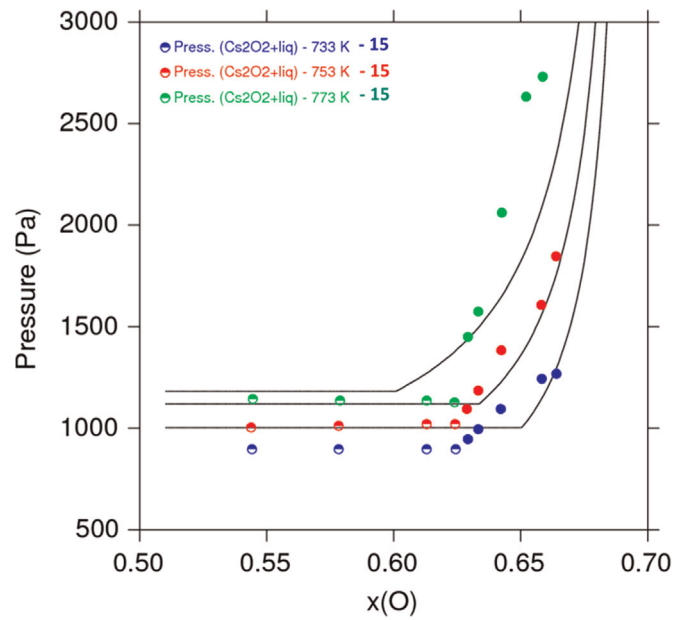


**Fig. 5.** Calculated pressure data versus composition in  $\text{Cs}_2\text{O}_2-\text{Cs}_2\text{O}$  region at 733, 753 and 773 K compared to the experimental data from Berardinelli [15].

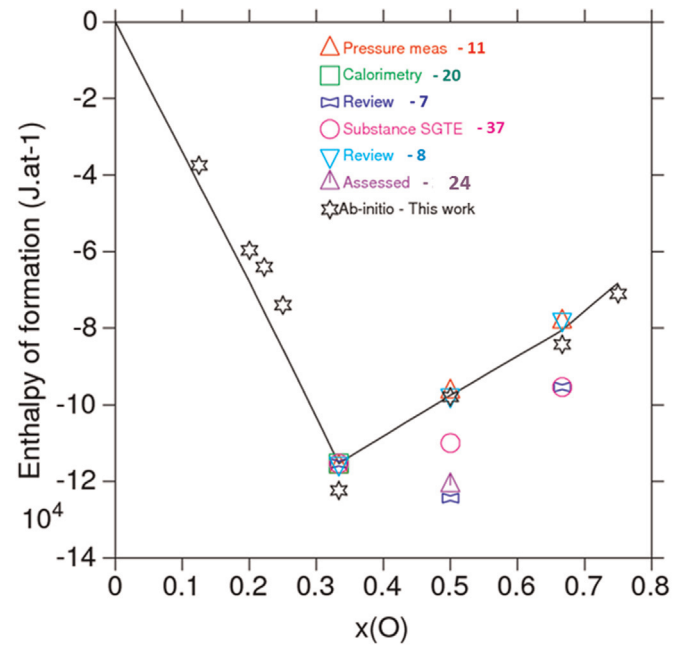


**Fig. 6.** Calculated enthalpy of formation for cesium oxides ( $\text{J}\cdot\text{mol}^{-1}\cdot\text{at}^{-1}$ ) compared to available literature data.

Berardinelli [16] or Knights and Phillips [11]. An attempt was made to fit these experimental pressure data measured in both (liquid+ $\text{Cs}_2\text{O}_2$ ) and liquid regions. As shown in Fig. 4(b), a very good agreement is found for the pressure data versus temperature in the (liquid+ $\text{Cs}_2\text{O}_2$ ) region. Pressure data obtained in both (liquid+ $\text{Cs}_2\text{O}_2$ ) and liquid regions versus oxygen composition at 733, 753, and 773 K melt are compared to experimental data measured by Berardinelli [15] in Fig. 5. The order of magnitude of calculated pressure is correct (around 10 % at 733 and 753 K). The deviation is higher at 773 K in the liquid where experimental issues are expected. As this region of the phase diagram is very uncertain and thermodynamic data are scarce, we chose to assess a minimum number of interaction parameters. New experiments

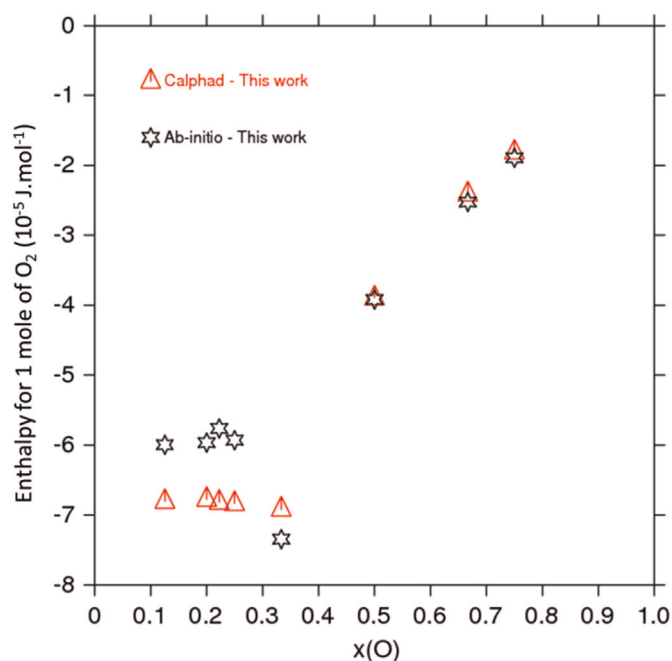


Fig. 7. Calculated enthalpy of formation of cesium oxides in  $\text{J} \cdot \text{mol}^{-1}$  of  $\text{O}_2$ .

Table 6

Mulliken charge for cesium and oxygen ions, population bond and length for oxygen–cesium bond, calculated with CASTEP code for the cesium oxides. Bond population may be used to assess the covalent or ionic nature of a bond. A high value of the bond population indicates a covalent bond, while a low value indicates an ionic interaction.

Oxide	Mulliken charge		Population bond O–Cs	Length (Å) O–Cs
	oxygen	cesium		
$\text{Cs}_7\text{O}$	–1.54	0.10–0.43	0.07	2.78091
$\text{Cs}_4\text{O}$	–1.54	0.10–0.68	0.10	2.96546
$\text{Cs}_{11}\text{O}_3(\text{Cs}_7\text{O}_2)$	–1.55	0.18–0.66	0.10	2.98298
$\text{Cs}_3\text{O}$	–1.53	0.51	0.06	2.90607
$\text{Cs}_2\text{O}$	–1.33	0.66	0.40	2.85277
$\text{Cs}_2\text{O}_2$	–0.81	0.81	0.22	2.96074
$\text{CsO}_2$	–0.44	0.88	0.00	2.97532
$\text{CsO}_3$	–0.46	0.90	0.00	3.23100

on both the phase diagram in the  $\text{Cs}_2\text{O}$ – $\text{CsO}_3$  composition range and on thermodynamic data for  $\text{Cs}_2\text{O}_2$ ,  $\text{CsO}_2$  and  $\text{CsO}_3$  would be very useful to better describe thermodynamics of the Cs–O system in this composition and temperature range.

Standard enthalpy of formation, entropy, and heat capacity data at 298.15 K for all oxide compounds are reported in Table 5 and compared to available information.

The calculated enthalpies of formation for all oxides are presented in Fig. 6 along side a comparison to available literature data. For  $\text{Cs}_7\text{O}$ ,  $\text{Cs}_4\text{O}$ ,  $\text{Cs}_7\text{O}_2$ , and  $\text{Cs}_3\text{O}$  compounds, there are no literature data. In the Gibbs energy function, the enthalpy and entropy terms (a and b) were assessed to reproduce the phase diagram data, namely the decomposition temperature. The enthalpy of formation data obtained by DFT was not used in the assessment. The final calculated enthalpy of formation data using the CALPHAD model are significantly lower (12–16%) compared to the calculated data using DFT. This disagreement has no simple explanation in terms of ab initio calculations. It could be attributed to the reference energy of the free atoms in relation to the pseudo-potential used to calculate the crystal cohesive energy, to the enthalpy increment between 0 K and the room temperature that the

thermodynamic model may overestimate. For  $\text{Cs}_2\text{O}$ ,  $\text{Cs}_2\text{O}_2$ ,  $\text{CsO}_2$  and  $\text{CsO}_3$  compounds, the agreement between CALPHAD and DFT data is excellent (0.5–6%). Both calculated data are consistent with experimental data from Settle [20] and Knights [11] for  $\text{Cs}_2\text{O}$  and from Knights [11] for  $\text{Cs}_2\text{O}_2$  and  $\text{CsO}_2$  and with the review by Cordfunke [8]. On the contrary, the assessed data by Lamoreaux and Hildenbrand [7], Lindemer [24] and in the Substance SGTE database [38] are underestimated.

For the standard entropy at 298.15 K for  $\text{Cs}_2\text{O}$ , the CALPHAD assessment reproduces selected experimental data from the calorimetric measurements by Flotow and Osborne [17]. The entropy derived from the pressure measurements by Berardinelli [15,16] is quite low in comparison to the value determined from calorimetry [17] whereas the calculated value by ab initio is 7% too high. More confidence was given to calorimetric measurements in agreement with Cordfunke [8]. For  $\text{Cs}_2\text{O}_2$  and  $\text{CsO}_2$ , only experimental data derived from vapor pressure data by Berardinelli [15,16] was available. The agreement is very good between assessed data of  $\text{Cs}_2\text{O}_2$  and reasonable for  $\text{CsO}_2$  and Knights [11]. Estimates by Cordfunke and Konings [8], Lamoreaux and Hildenbrand [7], Lindemer [24] are quite low compared to our assessed data as well as the entropy data derived from ab initio and quasi-harmonic approximation.

For the other oxide compounds, there are no experimental data. The assessed data with CALPHAD are systematically higher than DFT data.

The calculated heat capacity of  $\text{Cs}_2\text{O}$  at 298.15 K using CALPHAD or the DFT model is in good agreement with experimental data measured by Flotow [17], which gives a good confidence to the model coupling DFT and quasi-harmonic calculations.

Fig. 7 shows a different way to represent the calculated enthalpies of formation versus the oxygen mole fraction where these data are expressed in Joules for 1 mol of  $\text{O}_2$ . For the metallic compounds  $\text{Cs}_7\text{O}$ ,  $\text{Cs}_4\text{O}$ ,  $\text{Cs}_7\text{O}_2$  and  $\text{Cs}_3\text{O}$ , these enthalpies do not substantially change with composition. This is due to the fact that oxygen is sufficiently diluted so that the electronic structure of the metal is just slightly disturbed: the oxygen Mulliken charge varies very little throughout the series as shown in Table 6. This is not the case for the insulators  $\text{Cs}_2\text{O}$ ,  $\text{Cs}_2\text{O}_2$ ,  $\text{CsO}_2$  [25] and  $\text{CsO}_3$ . For these compounds, the oxygen–cesium bond population decreases and the cesium Mulliken charge increases from  $\text{Cs}_2\text{O}$  to  $\text{CsO}_3$  (Table 6) indicating an increasing ionicity. On the contrary, the oxygen–cesium covalency is decreasing. Thus the oxide  $\text{Cs}_2\text{O}$  is the most covalent compound, which is consistent as it is the most stable phase. It confirms the fact that there is no reason for  $\text{Cs}_2\text{O}_2$  to have a higher melting point than  $\text{Cs}_2\text{O}$  as stated previously.

New enthalpy of formation and heat capacity measurements would be very useful to better describe thermodynamics of the Cs–O system.

## 5. Conclusion

A review of available data on thermodynamics and phase diagram data of the cesium–oxygen system was first presented. Due to the lack of experimental thermodynamic data for the oxide compounds, ab initio calculations combined with a quasi-harmonic thermodynamic model were performed to estimate enthalpy of formation, standard entropy data and heat capacity data versus temperature for  $\text{Cs}_7\text{O}$ ,  $\text{Cs}_4\text{O}$ ,  $\text{Cs}_7\text{O}_2$ ,  $\text{Cs}_3\text{O}$ ,  $\text{Cs}_2\text{O}$ ,  $\text{Cs}_2\text{O}_2$ ,  $\text{CsO}_2$ , and  $\text{CsO}_3$  oxides. This approach was successfully applied and validated on the  $\text{Cs}_2\text{O}$  compound for which experimental data are available. Finally these calculated data coupled with available data coming from the literature were used to assess all the thermodynamic properties of the Cesium–Oxygen system using the CALPHAD method. A consistent thermodynamic description of this system was

obtained. The variation of thermodynamic data of the different oxides was related to their structural and bond properties investigated by ab-initio calculation. This work shows that the current approach combining CALPHAD and DFT/quasi-harmonic model is reliable and very useful, especially for such complex systems for which experiments are difficult. Nevertheless experimental information is still missing on the phase diagram and particularly on the melting point of  $\text{Cs}_2\text{O}_2$ , which could not be reproduced by our model and suggest future measurements are warranted. This model will be used to model higher order chemical systems such as Cs–U–O, Cs–Mo–O, etc., as representative for phases that form in irradiated oxide fuels in nuclear reactors.

## Appendix A. Supplementary material

Supplementary data associated with this article can be found in the online version at <http://dx.doi.org/10.1016/j.calphad.2015.02.002>.

## References

- [1] K. Konashi, T. Yato, H.H. Kaneko, *J. Nucl. Mater.* 116 (1983) 86.
- [2] C. Guéneau, B. Sundman, C. Chatillon, *J. Nucl. Mater.* 378 (2008) 257.
- [3] A. Berche, C. Rado, O. Rapaud, C. Guéneau, J. Rogez, *J. Nucl. Mater.* 389 (2009) 101.
- [4] A. Berche, N. Dupin, C. Guéneau, C. Rado, B. Sundman, J.-C. Dumas, *J. Nucl. Mater.* 411 (2011) 131.
- [5] C. Guéneau, N. Dupin, B. Sundman, C. Martial, J.-C. Dumas, S. Gossé, S. Chatain, F. De Bruycker, D. Manara, R.J.M. Konings, *J. Nucl. Mater.* 419 (2011) 145.
- [6] J.L. Flèche, *Phys. Rev. B* 65 (2002) 245116.
- [7] R.H. Lamoreaux, D.L. Hildenbrand, *J. Phys. Chem. Ref. Data* 13 (1984) 151.
- [8] E.H.P. Cordfunke, R.J.M. Konings, *Thermochemical Data for Reactor Materials and Fission Products*, Elsevier, North-Holland (1990) 92.
- [9] M.E. Rengade, *Compt Rend., Acad. Sci* 148 (1909) 1199.
- [10] G. Brauer, *Z. Anorg. Allg. Chem.* 255 (1947) 101.
- [11] C.F. Knights, B.A. Phillips, *J. Nucl. Mater.* 84 (1979) 196.
- [12] M. Blumenthal, M. Centerszwer, *Bull Intern. Acad. Pol. Cl. Sci. Math. Nat.* 1923 A (1933) 499.
- [13] I.I. Vol'nov, V.N. Belevskii, V.I. Klimanov, *Izv. Akad. Nauk SSSR Ser. Khim.* 7 (1967) 1411.
- [14] P. Touzain, *J. Ther. Anal.* 9 (1976) 441.
- [15] S.P. Berardinelli, Ph.D. thesis, University of Rhode Island, 1971.
- [16] S.P. Berardinelli, D.L. Kraus, *Inorg. Chem.* 13 (1974) 189.
- [17] H.E. Flotow, D.W. Osborne, *J. Chem. Thermodyn.* 6 (1974) 135.
- [18] G.V. Morris, Ph.D. thesis, University of Rhode Island, 1962.
- [19] M.N. Arnol'dov, M.N. Ivanovskii, G.N. Sereda, V.V. Stinikov, *Russ. Metall.* 4 (1975) 73.
- [20] J.L. Settle, G.K. Johnson, W.N. Hubbard, *J. Chem. Thermodyn.* 6 (1974) 263.
- [22] H. Okamoto, *J. Phase Equilib. Diffus.* 31 (2010) 86.
- [23] K.D. Hill, M. Gotoh, *Metrologia* 33 (1996) 307.
- [24] T.B. Lindemer, T.M. Besmann, *J. Nucl. Mater.* 100 (1981) 178.
- [25] J. Tai, Q. Ge, R.J. Davis, M. Neurock, *J. Phys. Chem. B* 108 (2004) 16798.
- [26] S. Gemming, G. Seifert, C. Mühle, M. Jansen, A. Albu-Yaron, T. Arad, R. Tenne, *J. Solid State Chem.* 178 (2005) 1190.
- [27] G. Brillant, F. Gupta, A. Pasturel, *J. Phys.: Condens. Matter* 21 (2009) 285602.
- [28] A. Jain, S.-A. Seyed-Reihani, C.C. Fischer, D.J. Couling, G. Ceder, W.H. Green, *Chem. Eng. Sci.* 65 (2010) 3025.
- [29] S. Riyadi, B. Zhang, R. de Groot, A. Caretta, P.H.M. van Loosdrecht, T.T.M. Pastra, G.R. Blake, *Phys. Rev. Lett.* 108 (2012) 217206.
- [30] S.J. Clark, M.D. Segall, C.J. Pickard, P.J. Hasnip, M.J. Probert, K. Refson, M. C. Payne, *Z. Krist.* 220 (2005) 567.
- [31] D. Vanderbilt, *Phys. Rev. B* 41 (1990) 7892.
- [32] J.P. Perdew, J.A. Chevary, S.H. Vosko, K.A. Jackson, M.R. Pederson, D.J. Singh, C. Fiolhais, *Phys. Rev. B* 46 (1992) 6671.
- [33] H.J. Monkhorst, J.D. Pack, *Phys. Rev. B* 16 (1977) 1748.
- [34] P. Villars, K. Cenzual, *Pearson's Crystal Data: Crystal Structure Database for Inorganic Compounds (on DVD)*, Release 2013/14, ASM International<sup>®</sup>, Materials Park, Ohio, USA, 2014.
- [35] F. Ortmann, F. Bechstedt, W.G. Schmidt, *Phys. Rev. B* 73 (2006) 205101.
- [36] A.T. Dinsdale, *SGTE data for pure elements, CALPHAD* 15 (4) (1991) 317.
- [37] M. Hillert, B. Jansson, B. Sundman, *J. Agren, Metall. Trans. A* 16 (1985) 661.
- [38] *SGTE Substances Database*, [www.thermocalc.com/TCDATA.htm](http://www.thermocalc.com/TCDATA.htm).
- [39] N. Beketov, *Bull. Acad. Sci. Russ.* 35 (1984) 541.